Journal of Catalysis 385 (2020) 300–312

Contents lists available at ScienceDirect

Journal of Catalysis

journal homepage: www.elsevier.com/locate/jcat

A temporal analysis of products (TAP) study of C_2-C_4 alkene reactions with a well-defined pool of methylating species on ZSM-22 zeolite

Evgeniy A. Redekop [a], Andrea Lazzarini [a,1], Silvia Bordiga [a,b], Unni Olsbye [a,*]

[a] Centre for Materials Science and Nanotechnology (SMN), Department of Chemistry, University of Oslo, P.O. Box 1126 Blindern, 0318 Oslo, Norway
[b] Department of Chemistry, NIS Centre and INSTM Center, University of Turin, via P. Giuria 7, 10125 Turin, Italy

ARTICLE INFO

Article history:
Received 9 December 2019
Revised 11 February 2020
Accepted 17 March 2020

Keywords:
Methanol-To-Hydrocarbons (MTH)
Temporal analysis of products (TAP)
ZSM-22
Dimethyl ether (DME)
Alkene methylation
Intrinsic kinetics
Surface methoxy species (SMS)

ABSTRACT

Reactions between alkenes and methanol or dimethyl ether (DME) on zeolite catalysts are involved in industrial processes that are highly relevant for the transition to renewable carbon sources, such as the Methanol-To-Hydrocarbons (MTH) process. In MTH chemistry, alkene methylation increases the length of product carbon chains, and its relative rate with respect to other reactions largely controls the overall selectivity. Experimental studies of alkene methylation present a considerable challenge because they are typically accompanied by cracking, hydrogen transfer, and aromatization reactions. Herein, the pulse-response Temporal Analysis of Products (TAP) methodology and complementary FTIR measurements were employed to isolate a well-defined population of surface species, consistent with Surface Methoxy Species (SMS) on Bronsted acid sites that are reactive in alkene methylation on a ZSM-22 (TON) zeolite. Their coverage was determined by TAP titration to be ca. 5% of the total amount of Brønsted acid sties, which was also indirectly suggested by FTIR data. C_2-C_4 alkenes were quantitatively reacted with SMS to precisely measure the intrinsic kinetic parameters of isolated alkene methylation steps. The rate constants increased and the activation energies decreased as functions of the carbon number (E_{C2H4} = 52 kJ/mol > E_{C3H6} = 32 kJ/mol > $E_{c\text{-}C4H8}$ = 16 kJ/mol). However, the rate constant for *iso*-butene was comparable to propene, despite its activation energy ($E_{i\text{-}C4H8}$ = 19 kJ/mol) being much lower than propene's. This effect is in agreement with the increased steric hindrance predicted by DFT for isobutene adsorption and methylation in TON zeolites. Our results considerably extend previously available TAP data on alkene methylation reactions and furthermore validate *ab initio* models of these crucial steps in the complex MTH chemistry on acidic zeolites.

1. Introduction

Precise kinetic characterization of a single reaction step in a complex catalytic mechanism is a fundamental challenge with profound implications in experimental physical chemistry. The catalytic performance of different materials and/or different operating conditions is typically compared based on steady-state turnover frequencies reflecting the global rates of multistep reaction sequences. However, more specific information about the intrinsic kinetics of individual reaction steps is needed in order to harvest the full potential of computational catalysis and advanced materials synthesis for rational catalyst design and optimization. Such data are highly desirable for single-parameter variation studies of structure-performance relationships and for benchmarking *ab initio* calculations of reaction rates [1,2]. Kinetic characterization of individual reaction steps is particularly challenging for zeolite-mediated hydrocarbon conversions, whereby several multistep reaction pathways usually co-exist and influence each other in a highly convoluted network [3–5]. To make matters even more intriguing, these complex reaction networks are strongly coupled to diffusion phenomena within the spatially non-uniform nanoporous media of a zeolite crystal [6,7]. Methanol-To-Hydrocarbons (MTH) provides a prominent example of a catalytic process affected by these complexities.

MTH has gained substantial scientific relevance as a flexible technology for converting fossil or renewable carbon sources into a variety of fuels and platform chemicals. Extensive research into the chemistry of MTH has indicated that the selectivity and stability of the process are intimately linked to the relative rates of methylation vs. cracking vs. hydrogen transfer reactions of alkenes and aromatics, which are controlled by the strength and number of

* Corresponding author.
E-mail address: unni.olsbye@kjemi.uio.no (U. Olsbye).
[1] Current address: Department of Physical and Chemical Sciences, University of l'Aquila, via Vetoio 42 (COPPITO 2) 67100 – l'Aquila, Italy.

https://doi.org/10.1016/j.jcat.2020.03.020
0021-9517/

acid sites, the framework topology, and operating conditions [8–10]. Conventional kinetic measurements, when extrapolated to zero contact time, may provide apparent rate parameters for specific reactions such as alkene and aromatics methylation [11–13]. Operando FTIR measurements, however, suggest that the resting state of the catalyst may vary substantially from one topology to another [14], thereby precluding systematic investigations of the relevant structure–activity correlations based on steady-state data. Furthermore, steady-state measurements cannot distinguish between the concerted (Eq. 1) and step-wise alkene (or arene) methylation pathways (Eq. 2a,b) that are predicted to dominate MTH kinetics under low and high temperature conditions, respectively[15–18]:

$$CH_3OR\ (R = H, CH_3) + C_nH_m + [^*H] = C_{n+1}H_{m+2} + ROH + [^*H] \quad (1)$$

$$CH_3OR\ (R = H, CH_3) + [^*H] = ROH + [^*CH_3] \quad (2a)$$

$$C_nH_m + [^*CH_3] = [^*H] + C_{n+1}H_{m+2} \quad (2b)$$

Theoretical methods have recently advanced to the point of being a viable alternative means to address these outstanding questions in zeolite catalysis [4,19,20]. Nevertheless, the validation of these theoretical methods likewise requires accurate estimates of pathway-specific kinetic parameters. Here, we report the rate coefficients and activation energies for a carefully isolated reaction in which an alkene molecule forms a C-C bond with a surface-bound methoxy group to produce an alkene with one extra carbon (Eq. 2b). This enhanced kinetic specificity is made possible by the judicial choice of a zeolite framework, the selection of pretreatment conditions leading to the formation of stable surface-bound methoxy species (SMS), and the use of a unique transient methodology for the kinetic characterization of well-defined catalyst states – Temporal Analysis of Products (TAP) [21].

The main objective of this study was to specifically elucidate the kinetics of individual reaction steps between alkenes and framework-bound methoxy groups. Therefore, the contribution from other possible methylating species to the observed kinetics, such as the hydrocarbon pool (HCP) species or methanol clusters within the nanopores, had to be minimized. The HCP species – both alkenes and aromatics – are initially formed during the autocatalytic period of the reaction from the (partially) equilibrated methanol/dimethyl ether (DME) mixture via the primary C-C coupling reactions. Once some of the HCP species are established, the formation of others inevitably follows, unless this is prevented by steric hindrances from the nanoscale confines of the host framework [22]. In order to simplify the sterically-allowed reaction network, experiments were performed with ZSM-22, a zeolite with a one-dimensional 10 member-ring pore system (4.6–5.7 Å diameter) of TON topology which precludes the formation of polycyclic and hexamethylated aromatics. Dimethyl ether (DME) was employed as a source of methyl groups rather than methanol because the latter is associated with increased rates of hydrogen transfer reactions, which in turn promote the formation of heavier hydrocarbon species [23–25]. DME was also advantageous from a practical point of view, since it is a gas under ambient conditions and is less likely to adsorb on non-catalytic surfaces within the equipment.

Reactions of ZSM-22 with DME and, subsequently, C_2-C_4 alkenes were investigated using the TAP technique which has been shown to produce highly specific kinetic information about the MTH process [17]. Complementary to TAP experiments, FTIR spectroscopy in a diffuse-reflectance cell was used to characterize the influence of DME pretreatment pressure on the state of the catalyst available for alkene methylation. The present study yields substantial new insights into the kinetic behaviour of alkene methylation reactions, which are discussed in the context of the latest modeling and experimental literature.

2. Experimental methods

2.1. Sample pretreatment and characterization

ZSM-22 with a nominal Si/Al ratio of 50 was acquired from Zeolyst International. As received sample was ion-exchanged three times for 2 h using a 1 M solution of NH_4NO_3 at 65 °C. The ion-exchanged zeolite was further calcined in static air at 550 °C for 5 h to desorb ammonia and yield the material in its protonic form. Standard characterization data for the resulting material are summarized in section 1 of the Supporting Information.

2.2. Temporal analysis of products (TAP)

TAP experiments were performed using a TAP-3E instrument (Mithra Technologies, USA) at the University of Oslo, which is equipped with an Extrel quadrupole mass-spectrometer. Gases were purchased from the following suppliers and used as received: Ne (4.5, AGA), C_2H_4 (2.8, Gerlink Holz + Co), C_3H_6 (2.5, AGA), i-C_4H_8 (2.0, Praxair), c-C_4H_8 (10% in Ar, Praxair), and DME (25% in Ar, Praxair). Alkenes were diluted with Ne as an inert standard in a 1:3 ratio, while the DME/Ar mixture was used without further dilution. For calibration purposes, a mixture of C_5H_{10} (2-methyl-2-butene, analytical standard, Sigma-Aldrich) and Ne was prepared by incrementally injecting several 100 μl doses of liquid pentene into an evacuated blending tank heated to 80 °C until no further rise of pressure was observed, after which the pressure was increased to the target level by Ne. The resulting 1:8 C_5H_{10}/Ne mix was delivered to the injection point via heated stainless steel lines to avoid condensation.

Sensitivities of the mass-spectrometer to different alkene fragments were determined for the standard 70 eV electron impact ionization settings by pulsing alkene/Ne mixtures of known compositions over quartz packing within the target temperature range of the reaction. Overlapping fragmentation patterns of alkenes showed general agreement with the NIST database [26] with minor deviations due to individual mass-spectrometer characteristics. For each alkene/Ne mixture, a standard set of AMUs was collected, i.e. 20.0, 26.0, 42.0, 56.0, 70.0, 84.0, which covered all expected methylation reagents and products (primary and secondary) in addition to the inert standard. Known relative sensitivity factors were later used for signal deconvolution. The absolute calibration coefficient of Ne was determined in a separate experiment by pulsing a large number (1000–2000) of pulses out of a small known volume (4 ml) until the pressure in the control volume dropped by approximately 10 kPa. The pulse size was estimated to be 5–10 nmol, well within the regime of Knudsen diffusion. Furthermore, the independence of the pulse shape from mixture compositions and from moderate variations of pulse intensity was confirmed in order to ensure a well-defined transport regime.

Samples of ZSM-22 were pressed into pellets with a Specac hydraulic press (2 tons) and sieved into a 250 < d < 420 μm fraction. Typically, 15–20 mg of this fraction was packed in the middle of a quartz tubular reactor (4 mm ID, 50 mm long) in the thin-zone configuration in order to maintain spatial uniformity of the sample. The rest of the reactor was packed with thoroughly washed and dried SiO_2 particles of the same size fraction. The tip of a K-type internal thermocouple was positioned within the sample layer. Temperature was controlled to within 0.5 °C by a Eurotherm temperature controller. Before measurements were performed, the sample was re-calcined *in situ* for 1 h at 550 °C in a 15 sccm flow

of synthetic air. The same calcination procedure was repeated between various series of measurements to regenerate the sample.

Adsorption characteristics of alkenes were investigated over freshly calcined, non-methylated ZSM-22 by injecting 50–100 pulses of alkene/Ne mixtures at various temperatures. The amount of pulses injected was adjusted to minimize the exposure of the catalyst to reagents, while ensuring that a sufficient signal-to-noise ratio was achieved for each AMU of interest by pulse averaging. In addition to the standard set of AMUs, potential oligomerization/cracking products were also monitored in selected experiments.

Then, to pre-treat the catalyst and create methylation-competent surface species, the sample was exposed to various amounts of DME using several alternative procedures: (i) long series of nanomolar pulses, (ii) low pressure (10^{-5} mbar) flow through a leak valve, or (iii) ambient pressure flow (10^{3} mbar) through a continuous flow valve. Following each pre-treatment, the reactor was evacuated to the base pressure of 10^{-8} mbar, while the background was continuously monitored with the mass-spectrometer. The methylation reactivity of the sample was probed at certain intervals during the post-DME evacuation by injecting a short series of nanomolar alkene pulses and monitoring their methylation products.

Once the standard protocol of DME pretreatment was selected (i.e. 3 min. of low pressure flow (ii) at 400 °C, followed by 2.5 h of evacuation), the kinetics of C_2-C_4 olefin methylation were quantified by injecting very short series (12 pulses each) of a reactant/inert mixture over the reference state of the DME-pretreated catalyst. Responses corresponding to the reactant, primary and secondary products as well as inert gas were monitored by the QMS. Temperature was varied in a randomized sequence between 300 and 400 °C in 25 pectroscopy was performed using a Bruker Vdegree steps. Therefore, the total amount of pulses injected to collect a full four-alkene/five-temperature dataset amounted to $12 \times 4 \times 5 = 240$ pulses. The subsequent titration experiments verified that the amount of methyl species removed from the catalyst surface within this dataset was smaller than 15% in comparison with the amount of methyl species prepared and stabilized on the surface during the pretreatment procedure, justifying the state-defining nature of kinetic measurements. The titration was performed by injecting propene pulses – the most reactive alkene – until the signals of its primary and secondary methylation products declined by at least a factor of five (ca. 1000 pulses).

Several data analysis techniques were used to interrogate the exit-flow rate transients. Bed-scale gas transport through the reactor was quantified based on inert responses at various temperatures (see Fig. S2). The inert transients were regressed using the finite-differences TAPFIT code [27] developed at the University of Gent. Both one-zone experiments with quartz-only packing and thin-zone experiments with the catalyst in place resulted in similar estimates of the Ne reference diffusion coefficient in quartz $^{273K}D_{Ne,\,SiO2} = 2.7{\cdot}10^{-3}$ m^2/s, while within the ZSM-22 layer it was estimated to be $^{273K}D_{Ne,\,ZSM\text{-}22} = 3.6{\cdot}10^{-4}$ m^2/s. An order of magnitude difference in reference diffusivities was caused by the increased void fraction and tortuosity within the layer of composite (macroporous) particles of ZSM-22. These parameters were fixed in all subsequent data analysis routines.

Attempts to model full transient responses of alkenes over non-methylated sample failed to capture their shapes adequately (see Figs. S5-S6), prompting us to apply alternative strategies for the analyses of alkene adsorption and methylation data. First, the Shekhtman reactivities method [28,29] was used to estimate the apparent equilibrium constants of alkene adsorption from the principal statistical moments of the exit-flow rate transients. Namely, the equilibrium constant (K_{eq}, m^3/mol) was evaluated for each alkene as

$$K_{eq} = \frac{[*C_nH_{2n+1}]}{[*H]C_nH_{2n}} = |r_1|\frac{\varepsilon L_{cat}A}{m_{cat}C_{H^+,tot}} \tag{3}$$

where ε is the void fraction (0.4), L_{cat} is the length of the catalyst zone in m, A is the reactor cross-section in m^2, m_{cat} is the catalyst mass loading in kg, $C_{H+,tot}$ is the total concentration of surface protons in mol/kg, and r_1 is the first reactivity (see Supporting Information, Section 2.2). This equation offers an intuitive interpretation of the r_1 reactivity coefficient in terms of familiar physico-chemical properties. Namely, for the simplest case of a reversible single site adsorption, r_1 is a dimensionless equilibrium constant, which is scaled in Eq. (3) according the nominal amount of free adsorption sites present in the volume of the catalytic zone per unit volume of the gas phase. For a more general interpretation of Shekhtman reactivities see section 2.2 of the Supporting Information.

Then, the transformation rates, gas concentrations, and surface uptakes of alkenes within the thin catalytic zone were reconstructed from the exit-flow rates via the kinetically "model-free" Y-Procedure [30–33]. Based on the reconstructed gas concentration transients, relative delays in the mean residence time of alkenes due to adsorption, Δτ, were estimated in relation to the mass-corrected mean residence time of diffusion-only inert responses:

$$\Delta\tau = \frac{(m_1/m_0)_{C_{TZ},ads} - (m_1/m_0)_{C_{TZ},diff}}{(m_1/m_0)_{C_{TZ},diff}} \tag{4}$$

where m_1 and m_0 are the first and zeroth moments of the gas concentration transients C_{TZ}, respectively. Finally, the following classical approximation of a first-order reaction in a completely mixed thin-zone TAP reactor was used to calculate the apparent rate constants of alkene methylation:

$$k_{app} = \frac{X}{1-X}\frac{1}{\tau_{res,corr}} \tag{5}$$

where the mean residence time in the catalyst zone ($\tau_{res,corr}$) was estimated based on the bed-scale diffusivity and then corrected to account for the observed adsorption-induced delay:

$$\tau_{res,corr} = (1+\Delta\tau)\varepsilon_b L_{TZ}L_{in2}/2D \tag{6}$$

2.3. Infrared spectroscopy

Diffuse Reflectance FT-IR (DRIFT) spectroscopy was performed using a Bruker Vertex 70 instrument equipped with a liquid nitrogen-cooled MCT detector and an *operando* "praying mantis" cell (Harrick Scientific Products Inc.). Each spectrum was obtained by averaging 128 scans with a resolution of 4 cm^{-1}. Approximately 40 mg of H-ZSM-22 (250 < d < 420 μm fraction) was loaded inside the "praying mantis" cell in a uniform layer. Pretreatment gases (O_2, Ar, DME) were supplied to the cell via calibrated mass-flow controllers. The outlet of the cell was connected to a three-way valve that directed the effluent either to the vent (during activation and ambient-pressure DME dosing) or to the vacuum system (during low-pressure DME dosing and evacuation). The sample was first activated in a 10 sccm flow of 20% O_2 in argon, while ramping the temperature from RT to 500 °C at 5 °C/min. After reaching the activation temperature, the sample was held at this temperature for 3 h. The cell was then flushed with pure Ar flow (10 sccm) for 30 min while cooling to 400 °C (reaction temperature) in order to remove O_2 before dosing DME. A flow of 10 sccm of 15% DME in Ar was delivered to the sample for 3 min either at P = 1 bar or P≈10^{-2} mbar. Afterwards, the sample was left under vacuum (P≈10^{-2} mbar) at 400 °C, while monitoring the spectral evolution for 150 min.

3. Results

3.1. Alkene transport and adsorption on non-methylated ZSM-22

Individual C_2-C_4 alkenes were pulsed over freshly activated ZSM-22 in the 100–400 °C temperature range. The injected molecules emerged from the microreactor unreacted ($m_{0,norm}$ = 1, see Fig. S3), confirming earlier reports [34,35] that in the limit of low coverage of active sites under the conditions of TAP experiments, alkenes do not measurably participate in dimerization, aromatization, or coke-producing reactions in zeolites. Mean residence times of alkenes in the reactor were considerably increased with respect to that of an inert tracer due to reversible adsorption. As an example, area- and time-normalized responses of ethene are shown in Fig. 1(a), where it can be seen that the ethene response broadens with decreasing temperature. The inset of the same figure depicts mean reactor residence times for the alkenes at different temperatures (see full responses for all alkenes in Fig. S4). These delays reflect the intrinsic rates of exothermic alkene sorption and, possibly, intraporous diffusion within a non-methylated ZSM-22 framework. Prior literature strongly suggests that Brønsted acid sites are the preferred alkene sorption sites, while silanol groups are unlikely to interact with short-chain alkenes [36–38]. For all temperatures, the extent of alkene delay followed the same order: C_2H_4< C_3H_6 ≈ i-C_4H_8< c-C_4H_8, which reflected the strength of their adsorption within the zeolite.

The apparent equilibrium constants of alkene adsorption were estimated from alkene responses using the Shekhtman reactivities method [28,29] – an established method of TAP data analysis based on statistical moments of exit-flow rate transients. The corresponding van 't Hoff plots and estimated thermodynamic quantities are shown in Fig. 1(b) and Table 1, respectively. For linear alkenes, as expected, the apparent equilibrium constant increases with the carbon number at each temperature. Isobutene, however, is adsorbed less strongly than 2-butene and even slightly less strongly than propene. Van 't Hoff dependencies of the apparent adsorption constants for all alkenes except ethene exhibited pronounced deviations from the expected exponential behavior, which can already be seen qualitatively from the mean residence time plots in Fig. 1A.

One possible explanation for the non-linearity of van 't Hoff plots is the manifestation of intra-porous diffusion. Molecular Dynamics (MD) simulations [39] suggest that in the limit of zero loading, self-diffusivities of C_2-C_4 alkenes in the pores of non-methylated ZSM-22 are on the order of 1-5e^{-8} m^2/s for the 300–400 °C temperature range. According to the sensitivity studies of typical TAP experiments [40], the characteristic time of intraporous diffusion at this rate is negligible with respect to the characteristic time of bed-scale Knudsen diffusion. Thus, the adsorption and reaction kinetics are expected to follow zero-dimensional mean-field microkinetics devoid of intra-porous concentration gradients. A simple model of single-site reversible adsorption was used in an attempt to describe the shapes and temperature evolution of alkene responses, but this model could not adequately capture the data (see Fig. S5). Furthermore, a two-parameter model [40,41] with explicit intraporous diffusion also failed to produce satisfactory results (see Fig. S6). These unsuccessful attempts to model the full transients along with the curvature of van't Hoff plots in Fig. 1(b) suggest that the process of alkene adsorption on ZSM-22 involves more complex mechanisms than these simple adsorption/diffusion models can account for.

In the absence of a reliable explicit model, the adsorption data were evaluated using a kinetically "model-free" method – the Y-Procedure [30–33]. In brief, instantaneous gas concentrations $C_{TZ}(t)$, mol/m^3 and adsorption rates $R_{TZ}(t)$, $mol/kg_{cat}/s$ of each alkene within the uniform thin zone of ZSM-22 were reconstructed from their exit-flow rate transients by a frequency-domain algorithm that extracts purely kinetic dependencies from the reaction–diffusion data. Instantaneous alkene uptakes within the catalyst $U_{TZ}(t)$, mol/kg_{cat} were also calculated as time-dependent integrals of the reconstructed adsorption rates. The temporal evolution of reconstructed quantities (see Fig. 2) appears to be consistent with the expected general features of a fully-reversible process [32]. Namely, the gas concentration and surface uptake pass through a maximum and then decay to zero by the end of the curve. The rate transient passes through a maximum, then crosses zero at the point of Momentary Equilibrium (ME), and finally decays to zero in the negative semi-plane. However, examination of these quantities in the three-dimensional kinetic space, i.e. {$C_{TZ}(t)$, $R_{TZ}(t)$, $U_{TZ}(t)$}, demonstrated that, in agreement with other analysis methods, they exhibit significant deviations from a simple model of a state-defining experiment with a single-site adsorption (see Fig. S7). To the best of our knowledge, this constitutes the first example of the Y-Procedure applied to adsorption on microporous materials.

Despite lack of agreement between simple models and experimental adsorption data, the reconstructed rate-concentration transients provide essential information for the kinetic analysis of alkene methylation data. These transients enabled empirical quantification of the additional alkene residence times within the catalytic sample due to their reversible adsorption on free Brønsted protons, which were identified as the most abundant surface intermediates under the conditions of these kinetic measurements (see Section 3.3). The apparent relative delay due to adsorption was estimated by comparing the time at which the mean thin-zone concentration occurs in the presence and in the absence of adsorption. The thin-zone concentration transients for ethene with and without adsorption, the latter being derived from the response of an inert gas, are compared in Fig. 2(b) at 350 °C. As highlighted in the figure, the mean time of the gas concentration transient with adsorption differs by almost a factor of two from the mean time of the adsorption-free concentration transient. Other alkenes were also delayed by adsorption longer than expected from purely diffusive response, by up to five times at 300 °C. The empirical relative delays with respect to the adsorption-free expected value, i.e. $\Delta\tau$, were later used to correct the diffusional residence times in the catalyst zone when estimating the kinetic constants from the methylation data.

3.2. DME pre-treatment: Establishing a well-defined population of surface-bound methoxy species (SMS)

The main objective of this study was to specifically elucidate the kinetics of individual reaction steps between alkenes and framework-bound surface methoxy species (SMS) via the stepwise methylation pathway (Equation 2). Under ambient flow conditions, multiple species containing a methoxy group are present within the nanopores of zeolites that can react with an alkene substrate and transfer a methoxy group, such as DME, methanol, methanol dimers adsorbed on Brønsted acid sites, or HCP species that emerge *in situ* from the reactants. These species can be termed methylation-competent, as opposed to other methoxy-containing species that are not reactive towards alkenes, such as DME or methanol adsorbed on isolated silanol groups in MFI silicalite [25,42]. TAP experiments in the low-pressure regime have an advantage over conventional measurements because the population of the aforementioned species can be minimized, thereby enhancing the contribution of vacuum-stable SMS to the observed product formation.

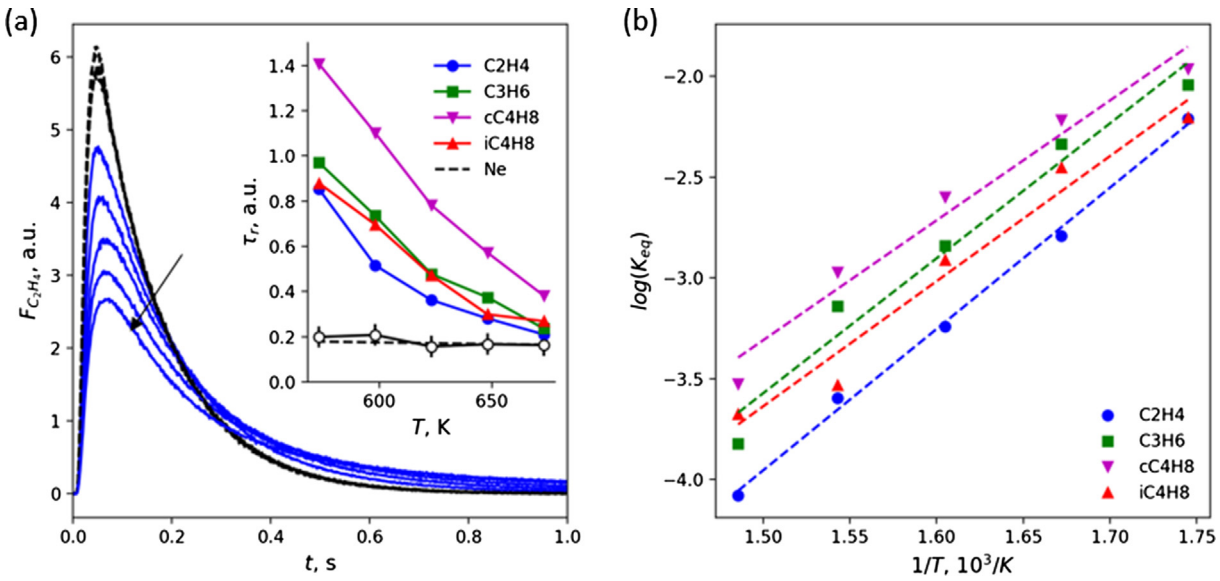

Fig. 1. Alkene responses over non-methylated ZSM-22 zeolite: (a) Area- and time-normalized (i.e. corrected for the molecular mass) responses for C_2H_4 at different temperatures (blue) compared to Ne (black dashed). The arrow indicates the progression of decreasing temperature from 400 to 300 °C (673–573 K). The inset shows the mass-corrected mean reactor residence time for all gases as a function of temperature. Ne data contain error bars (one standard deviation) to indicate the scale of measurement uncertainties. The black dashed line in the inset corresponds to the expected square-root dependency of the Ne residence time. (b) Apparent adsorption equilibrium constants for C_2-C_4 alkenes on non-methylated ZSM-22 in van 't Hoff coordinates ln(K_{eq}) vs. 1/T. The dashed lines correspond to a linear fit.

Table 1
Estimated thermodynamic parameters of alkene adsorption on non-methylated ZSM-22.

alkene	$-\Delta S_{ads}$, J/mol/K	$-\Delta H_{ads}$, kJ/mol
C_2H_4	120	58
C_3H_6	113	56
c-C_4H_8	102	49
i-C_4H_8	108	52

In this study, DME was employed as a source of methoxy species instead of methanol because the latter is associated with increased rates of hydrogen transfer reactions, which in turn promote the formation of the hydrocarbon pool and coke precursors [22,25,43]. Initial experiments employed the pulsing protocol from Brogaard et al. [17] whereby a methylating agent was injected in pulse-pairs with an alkene until a stable conversion of alkene per pulse was reached at a given temperature. In a typical DME/alkene pulse pair, neither methylated alkene products nor DME could be detected above the background signal during the DME pulse (see Fig. S8), which confirmed that the products seen during the alkene pulse were formed predominantly by the direct methylation of an injected alkene instead of the HCP-mediated reactions. In fact, the formation of alkenes from DME could be induced only by drastically enhanced exposures to DME, either as a result of many thousands of DME pulses or a 20-fold increase in the amount of DME molecules injected per pulse (see transients with enhanced intensity in Fig. S8).

Unreacted DME was observed slowly desorbing from the catalyst surface as indicated by a rising background signal at amu 45 (see Figs. S9-S10). Similar extremely slow rates of desorption were observed for methanol and water, precluding qualitative evaluation and quantitative analysis of oxygenates. Continuously desorbing DME could lead to various undesirable side processes including the obstruction of alkene diffusion in the micropores as well as alkene methylation via the concerted pathway (Scheme 1). Therefore, the pretreatment protocol was adjusted in order to separate in time the establishment of the SMS population and their reactions with incoming alkene reagents.

3.2.1. Ambient vs. low-pressure DME pre-treatment

The partial pressure of DME and the rate of the catalyst's exposure to DME were varied in order to establish a stable and reproducible SMS population on the catalyst surface. Two stable states with differing reactivity were identified in these experiments

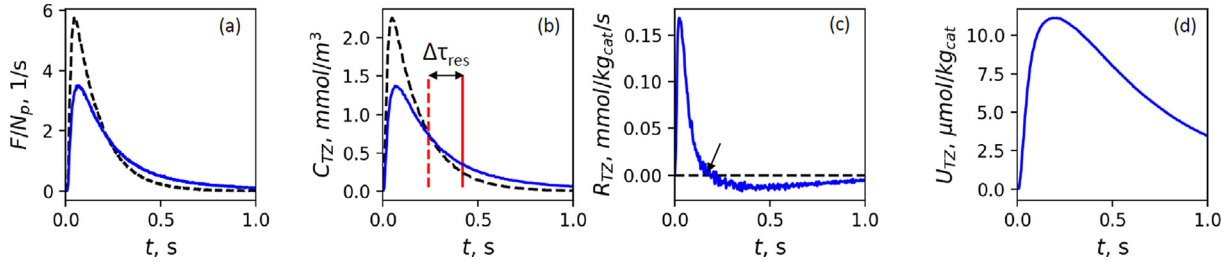

Fig. 2. Reconstruction of kinetically "model free" transients within the thin catalyst zone during an ethene injection at 350 °C: (a) original area-normalized exit-flow rates, 1/s; (b) gas concentrations, mol/m^3 and (c) transformation rates, mol/kg_{cat}/s within the thin catalyst zone obtained via the Y-Procedure, and (d) surface uptake of adsorbed alkene, mol/kg_{cat} obtained from the transformation rate by integration in time. Blue solid lines – C_2H_4, black dashed lines – Ne. The time axis is mass corrected in all images. The mean gas concentration times of ethene and inert as well as their difference are indicated in panel (b) to highlight the adsorption-induced delay. The point of Momentary Equilibrium (ME) is shown by the arrow in panel (c).

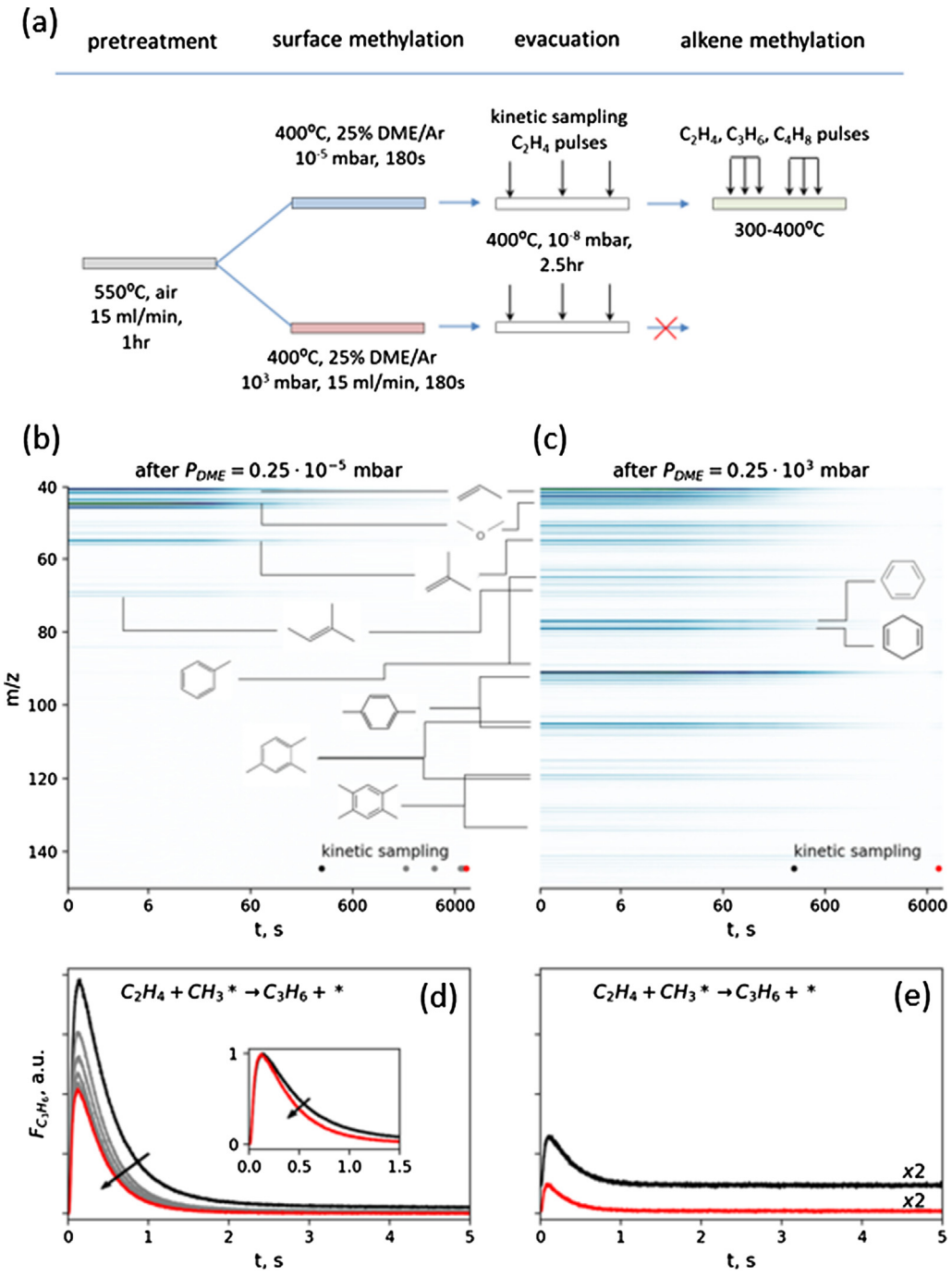

Fig. 3. DME pre-treatments of ZSM-22 to establish a well-defined reference state for kinetic measurements: (a) Experimental protocols used to compare the pretreatment regimes; (b) and (c) Time-resolved mass-spectra collected during the post-DME evacuation period. The color intensity (from white to deep blue) corresponds linearly to the intensity of mass-spectra in arbitrary units. The time points at which ethene was injected to probe the catalyst's methylation reactivity (kinetic sampling) are indicated by circular markers; (d) and (e) Propene responses during ethene injections (black – first pulse, gray – intermediate pulses, red – the last pulse). The inset of panel (d) shows height-normalized propene responses to highlight the evolution of their shapes during the evacuation. The arrows indicate the progression of evacuation time. In panel (e), the propene signal is magnified twofold in order to clearly represent the data on the same vertical scale as in panel (d).

corresponding to low- and ambient-pressure DME pretreatments at 400 °C, respectively (Fig. 3(a)). In each case, the catalyst was subjected to a short (180 s) continuous flow of 25% DME in Ar, either at a total pressure of 1 bar (ambient flow) or at 10^{-5} mbar (low-pressure flow). After this brief DME exposure, in both cases the catalyst was rapidly evacuated by connecting the reactor exit to the vacuum chamber with a background pressure of 10^{-8} mbar. At various stages of evacuation, the intrinsic methylation reactivity of the catalyst was probed by injecting nanomolar pulses of ethene and quantifying the amount of propylene produced. Time-resolved background mass-spectra following evacuation are shown in Fig. 3 (b) and (c) for the low-pressure and ambient-pressure DME exposures, respectively. The ambient-pressure pretreatment resulted in the formation of multiple characteristic MTH products, including light alkenes and substituted mono-aromatic species, which slowly desorbed from the catalyst along with unreacted DME. The low-pressure pretreatment, on the other hand, produced mostly C_2-C_6 alkenes and unreacted DME without significant quantities of

aromatics. In both cases, residual hydrocarbons could still be detected after 2 h of evacuation, albeit in very small amounts.

Ethene injections during the post-pretreatment evacuation revealed substantial differences in the methylation reactivity of the resulting catalyst states (Fig. 3(d-e)). Propylene that was initially produced from the residual DME was observed as a constant raised background, which dominated over propylene production from the injected ethene in the case of atmospheric-pressure pretreatment, but not in the case of low-pressure pretreatment. Two and a half hours after evacuation, the residual methylation reactivity of the catalyst stabilized. The total propylene yield declined for both pretreatments, and the background of DME as well as all hydrocarbons returned to a baseline of zero, indicating that all methylation activity and desorption had stopped. Surprisingly, much less propylene was produced from injected ethene after the evacuation in the case of ambient-pressure DME treatment compared to the case of low-pressure treatment. The substantial difference in residual, post-evacuation reactivity suggests that more SMS survive the pretreatment/evacuation procedure in the case of low DME pressure. Concurrently with reactivity stabilization upon prolonged evacuation, propylene responses after low DME pressure became progressively narrower until they converged to a stable shape, as depicted in the inset of Fig. 3(d). Comparable residual reactivity and pulse shape were obtained in experiments where DME was injected in the form of hundreds of nanomolar pulses, rather than a 3-minute low-pressure flow through a leak valve (see Fig. S11). Prolonged evacuation was still required in the case of pulse-wise exposure to DME to allow for complete DME desorption from the catalyst, making the entire pulse-wise pretreatment procedure unreasonably long and less favorable than the low-pressure flow pretreatment.

Overall, combined mass-spectrometric (TAP) and complementary spectroscopic (IR) observations (Section 3.2.2.) motivated the selection of the standard pre-methylation protocol that was used in all subsequent kinetic measurements: low-pressure DME flow at 400 °C for 3 min, followed by evacuation for 2.5 h at the same constant temperature. The resulting reference catalyst state was still active for alkene methylation after an overnight evacuation at 400 °C.

3.2.2. IR characterization of DME-treated ZSM-22

The ambient- and low-pressure exposures of the catalyst to DME flow were repeated in IR experiments to gather complementary data on the resulting state of the catalyst surface. Due to the technical limitations of the IR setup, the low-pressure results were obtained at 10^{-2} mbar DME flow instead of 10^{-5} mbar employed in the actual TAP experiment. Consequently, the corresponding IR data are indicative of general trends, rather than a quantitative comparison to TAP conditions. DME exposure caused pronounced changes in the two main spectral regions of interest – the O-H region (3400–3800 cm^{-1}) and the C-H region (2600–3300 cm^{-1}). It is well known from the literature [14,44,45] that MTH processes in zeolites give rise to very convoluted *in situ* IR spectra which are difficult to interpret. Therefore, the present discussion is focused on the hydroxyl region, while a limited interpretation of the C-H region is provided in section 3 of the Supplementary Information.

DRIFTS spectra of H-ZSM-22 before and after its interaction with DME at 400 °C are shown in Fig. 4(a) for 10^{-2} mbar and in Fig. 4(b) for 10^{3} mbar exposures to DME flow, followed by continuous evacuation at 10^{-2} mbar. The numbered O-H vibrations in both panels can be identified as follows [46,47]: i) signals 1–2 centered at 3735 and 3690 cm^{-1} correspond to two different families of silanol groups (Si-OH-Si) respectively; ii) signal 3 centered at 3585 cm^{-1} is from Brønsted-type acid protons (Si-OH-Al); iii) signal 4 across the entire ν_{OH} region (3800–3300 cm^{-1}) and centered at 3525 cm^{-1} is due to the hydrogen bond-like interaction between the aforementioned protons and O atoms of the surrounding framework.

Silanol groups present in the catalyst respond in a similar way to both pressure regimes. Upon exposure to DME, external silanols (signals 1 in Fig. 4 (a) and (b)), which are more accessible, are rapidly covered by the reactant [47], as testified by the sudden

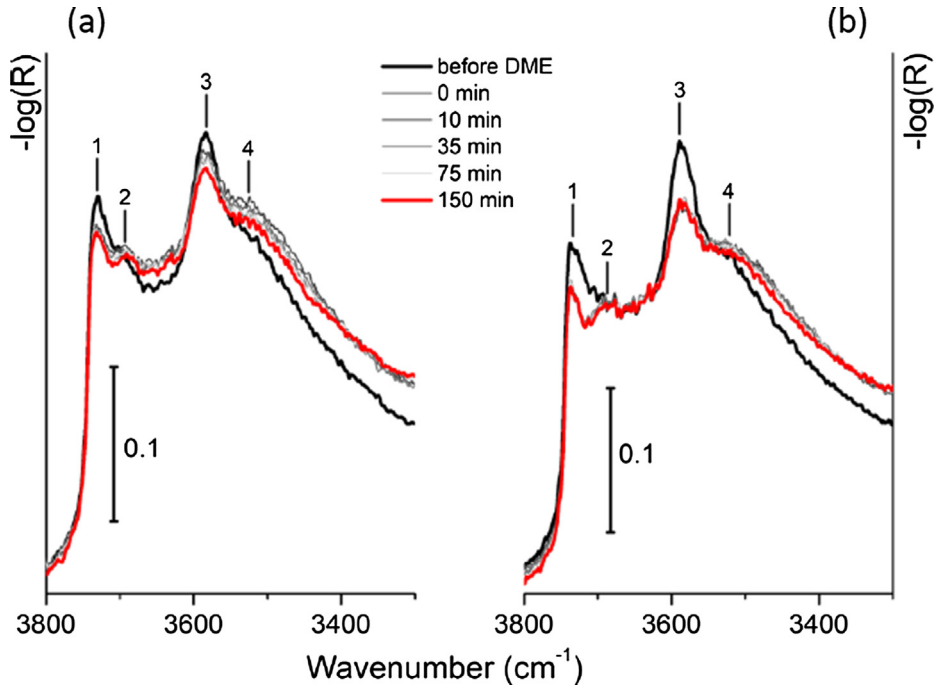

Fig. 4. Magnification of the O-H stretching region (3800–3300 cm^{-1} - ν_{OH}) for the H-ZSM-22 sample exposed to DME flow at P≈10^{-2} mbar (a) and P = 1 bar (b) after 0, 10, 35 and 75 min of evacuation at P≈10^{-2} mbar (grey scale). The catalyst prior to the exposure to DME is depicted with the thick black line, while the final state after 150 min of evacuation is depicted with the thick red line.

decrease of the peak at 3735 cm^{-1}; however, not all of the protons interact with DME due to the high temperature at which the reactant is dosed. Instead, inner silanols (signals 2 in Fig. 4 (a) and (b), 3690 cm^{-1}), which arise from crystal defects and are located in less accessible positions, remain unaltered. After this initial change, no other evolution were appreciable for these two silanol sites during the 150 min of evacuation.

Brønsted acid sites, unlike silanols, exhibited different behavior in the two pressure regimes of DME exposure. Under the ambient pressure regime (Fig. 4(b)), a trend similar to silanol species was observed, i.e. as soon as DME was dosed, signal 3 suddenly decreased and remained stable during the entire 150 min of evacuation under dynamic vacuum. Under the low-pressure regime (Fig. 4(a)), there was a gradual change in signal 3, indicating a continuous slow consumption of acidic protons. Similar behavior was observed for signal 4 corresponding to the hydrogen bonding of Brønsted protons with the surrounding framework oxygen atoms. Importantly, the IR data reveal that the residual amount of Brønsted protons remains relatively high and close to their original concentration after low-pressure DME exposure, suggesting that surface methoxies are likely to exist as minority species in the reference catalyst state during TAP measurements.

3.2.3. Estimating SMS coverage in the reference catalyst state

The IR spectra after the standard low-pressure DME pretreatment revealed a considerable residual signal of free protons and a clear trend of decreasing amounts of surface species with aliphatic C-H, suggesting that the population of methoxy species in the reference catalyst state is much lower than a theoretical monolayer. To quantitatively estimate SMS coverage available for alkene methylation in the reference state, a titration TAP experiment was performed in which a long sequence of propene pulses was issued to gradually remove methoxy species from the DME-pretreated catalyst surface at 400 °C. The apparent rate constant of propene consumption during this titration sequence is shown in Fig. 5 as a function of the amount of carbon removed from the catalyst. It

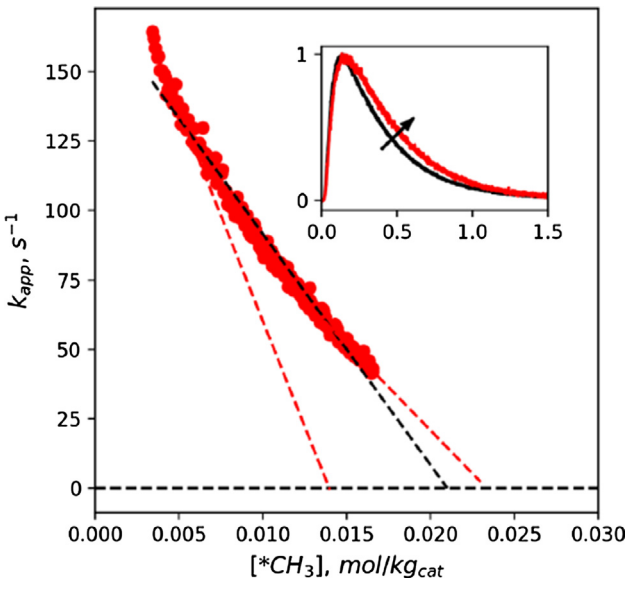

Fig. 5. TAP titration of SMS from the reference state of ZSM-22 at 400 °C. The apparent rate constant of butene production k_{app}, s^{-1} during propene pulses is plotted vs the amount of carbon removed [*CH_3], mol/kg_{cat}. Dashed lines indicate linear fits to (red) the first 20 and last 100 data points or (black) to the entire dataset. The inset highlights the evolution of the butene response shape (height-normalized) between the beginning and the end of the titration sequence.

should be noted that the shape of the product response becomes slightly broader with decreasing methoxy coverage, as highlighted in the inset of Fig. 5, which can be explained by the increasing availability of free protons that delay the outgoing alkene molecules.

The rate constant expectedly decayed as more and more methoxy species were removed. The simplest kinetic model would suggest that the apparent constant is linearly proportional to the surface concentration of SMS:

$$k_{app} = k_{int}[*CH_3] \quad (7)$$

Extrapolation of this line to the intersection with the abscissa should yield the total amount of methoxy species available in the reference state before the start of the titration sequence. Although the dependency in Fig. 5 deviates from a straight line, it does provide a useful estimate of the initial methoxy coverage in the range of 0.014–0.023 mol/kg_{cat}. This coverage constitutes 4–6% of the total concentration of Brønsted acid sites.

The <10% cap on the available coverage of methoxy species in combination with the abundance of protons in the IR spectra of the reference state justify an essential assumption that had to be made about the residence time within the catalyst zone in order to estimate the apparent constants of alkene methylation. Namely, it was assumed that alkene molecules adsorbed on free protons constitute the most abundant surface species ($\gg$10%) during alkene methylation compared to the minority (<10%) of the surface methoxy species. Thus, relative delays in the mean catalyst residence times that were empirically-derived from adsorption transients over non-methylated catalyst (see section 3.1) with 100% free protons could be used to correct the expected diffusion-only mean residence time in the catalytic zone during methylation experiments.

3.3. Kinetics of alkene methylation steps

C_2-C_4 alkenes were reacted with ZSM-22 in a pre-methylated reference state at 300–400 °C to investigate the intrinsic kinetics of isolated methylation steps. Typical response curves for ethene injections are shown in Fig. 6(a) including curves for the reactant, primary, and secondary products. Although minor amounts of tertiary products could also be detected with increased amplification gain, only the primary and secondary methylated alkenes were considered in the analysis. Ethene was irreversibly converted into propene, which is reflected by the missing area between ethene and neon curves in the peak of the pulse. Later, the ethene transient exhibited a longer tail that intersected the neon curve around 0.4 s. This shape is consistent with the delay caused by a parallel reversible adsorption on abundant Brønsted acid sites. Product responses exhibited similar tailing features, which broadened at lower temperatures.

The formation of primary and secondary methylation products from ethene increased steeply with temperature (inset of Fig. 6 (a)), which was also observed for other alkenes (see Fig. S12). The rate constants of the primary methylation step for each reactant were calculated based on the combined yields of primary and secondary products, since products were monitored with increased mass-spectrometer sensitivity to compensate for relatively low overall conversion levels. The resulting apparent rate constants followed linear dependencies in the Arrhenius coordinates (Fig. 6(b)) with determination coefficients R^2 above or close to 0.99. In agreement with theoretical predictions and TAP data [17], alkene reactivity towards SMS increased from ethene to propene to linear butene, while isobutene exhibited a lower rate constant than propene. Table 2 summarizes the rate constants and

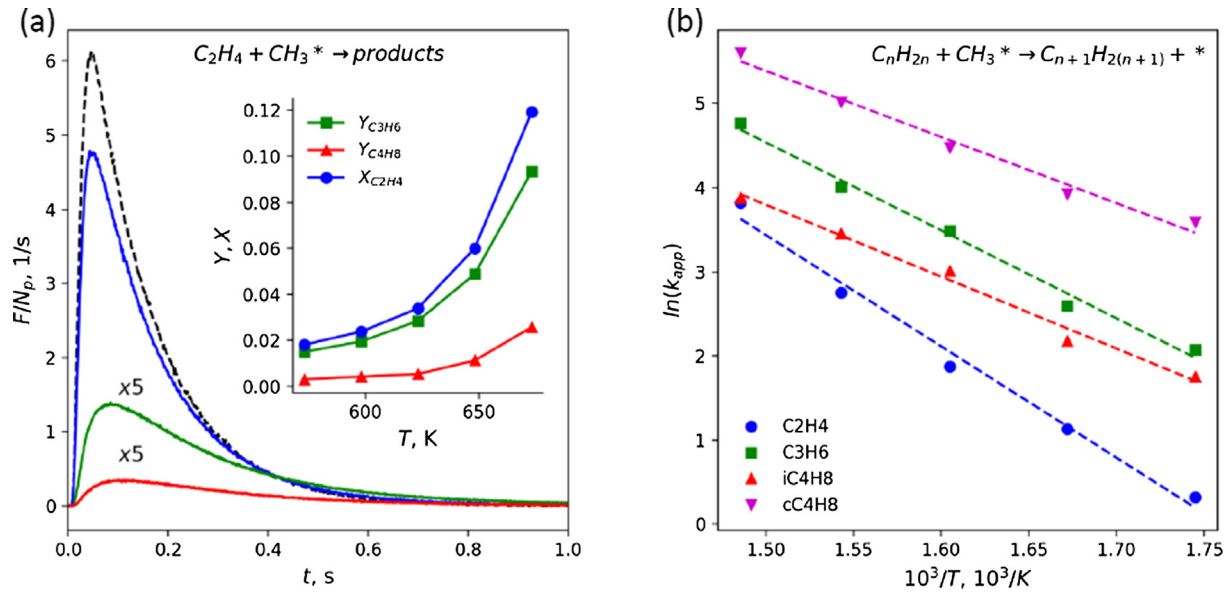

Fig. 6. (a) Area-normalized, mass-corrected exit-flow rate transients F/N_p, s^{-1} of Ne, C_2H_4, C_3H_6, and C_4H_8 during C_2H_4 methylation by DME-pretreated ZSM-22 at 400 °C (673 K). The inset shows the yields of primary and secondary products along with the total conversion of the reactant for all temperatures; (b) Apparent rate constants of alkene methylation k_{app}, 1/s in Arrhenius coordinates, i.e. log(k) vs 1/T. Linear fits are shown as dashed lines.

Table 2
Estimated apparent kinetic parameters of alkene methylation.

alkene	k_{app}, 1/s at 673 K	ΔE_{act}, kJ/mol
C_2H_4	45	110
C_3H_6	117	88
i-C_4H_8	49	71
c-C_4H_8	271	65

estimated activation energies, which are discussed in the context of existing literature in the following section.

4. Discussion

The experimental findings presented in this work pertain to three processes that were investigated separately: (1) the interactions of C_2-C_4 alkenes with the H-form of ZSM-22 zeolite, (2) the reactions of dimethyl ether (DME) on the zeolite, and (3) the subsequent reactions between alkenes and the surface methoxy species (SMS) surviving on the zeolite after a short DME exposure.

Experimental measurements of alkene adsorption parameters on acidic zeolites are nearly absent in existing literature, primarily due to the methodological difficulty of isolating the adsorption step from subsequent reactions such as oligomerization and/or cracking. Sarazen and Iglesia reported [48] adsorption equilibrium constants for C_2-C_4 alkenes over a TON zeolite at 230 °C, which were derived either from variable-pressure IR measurements or, indirectly, from the steady-state kinetics of alkene dimerization. According to their data, the adsorption strength increases with the carbon number for linear alkenes, while *iso*-butene is adsorbed more weakly than linear butene due to significant confinement effects of the pore walls. In principle, the TAP method is uniquely suited for more direct measurements of adsorption characteristics for alkenes because the probability of dimerization reactions is minimized at extremely low pore occupancies. Nevertheless, TAP literature has not previously provided much information about alkene adsorption in zeolites. Batchu et al. report [34,49] that ethene responses over H-ZSM-5 at 200–300 °C conformed to the shape expected from a single-site reversible adsorption model and could be described well by *ab initio* predicted thermodynamic parameters [50]. Other available TAP data on 10MR microporous materials primarily concern alkane adsorption in non-acidic MFI silicalites [51,52].

In general agreement with these references, we observed that linear hydrocarbons with longer carbon chains spent more time within the zeolite (inset of Fig. 1(a)). Similarly to propene, *iso*-butene had a lower residence time within the material than linear butene, reproducing the results of Sarazen and Iglesia [48]. The apparent adsorption equilibrium constants (Fig. 1(b)) estimated via moment analysis reflected the same trends. The ethene adsorption parameters reported herein, i.e. $-\Delta H_{ads}$ of 58 kJ/mol and $-\Delta S_{ads}$ of 120 J/mol/K, were generally similar to those reported for ZSM-5 by Alexopoulos et al. [50], i.e. $-\Delta H_{ads}$ of 48 kJ/mol and $-\Delta S_{ads}$ of 99 J/mol/K. These slightly higher observed values could be related to the differences between TON and MFI topologies. However, the shapes of the curves could not be captured by simple models with reversible adsorption or porous diffusion, suggesting the involvement of more complex adsorption/diffusion mechanisms. Likewise, the thermodynamic parameters estimated from the apparent equilibrium constants (Table 1) did not behave as expected for homologous alkenes on an acidic zeolite.

Hydrocarbon adsorption in zeolites is expected to strengthen for linear hydrocarbons with longer carbon chains (e.g. for alkanes see De Moor et al. [53] and for alkenes see Sarazen and Iglesia [48] and Cnudde et al. [54]). The increasing adsorption enthalpies of homologous alkanes on acidic ZSM-5 (e.g. 50 kJ/mol for butane to 70 kJ/mol for hexane in Keipert and Baerns [40]) reveal that TAP data generally reproduce these expected trends for hydrocarbon adsorption in zeolites. Theoretical models predict that homologous linear C_2-C_4 alkenes in acidic TON zeolites like ZSM-22 should gain 10–15 kJ/mol in adsorption enthalpy per carbon [48,54], reaching close to 100 kJ/mol for physisorbed and π-bonded isobutene in ZSM-22 [55]. Contrary to this expectation, we observed that the enthalpy remained relatively constant around 50 kJ/mol. This observation can be interpreted as a sign that under these specific conditions the majority of alkene molecules entering the ZSM-22 pores exist in a relatively weakly bound state, the energy of which does not differ significantly among homologues. Based on observations reported in the literature [36–38],

it is unlikely that alkene adsorption on silanol groups plays a significant role in comparison with adsorption on the Brønsted acid sites. Two-site adsorption models, e.g. adsorption on proximal vs. isolated Brønsted sites [36], and anomalous intraporous diffusion mechanisms provide possible extensions for the alkene adsorption/diffusion modeling of TAP responses in further research. Despite a persisting gap in our understanding of alkene adsorption and diffusion in ZSM-22, the alkene responses over this non-methylated surface provide empirical measures of the delay in the mean residence time induced by adsorption and of the scale of the apparent adsorption enthalpy, both of which are required subsequently for the interpretation of alkene methylation kinetics.

Unlike alkene adsorption in the limit of zero coverage, the interaction of zeolites with methylating oxygenates (DME and methanol) at elevated temperatures inevitably leads to chemical reactions, starting from the formation of surface methoxy species and ultimately leading to MTH. The main distinguishing feature of ZSM-22 in the context of MTH chemistry is the steric hindrance that its relatively narrow 1D 10MR channels exert on the hydrocarbon pool (HCP) species, leading to a well known prevalence of the alkene-driven methylation cycle over the aromatics-driven cycle during steady-state operation [56,57]. Previous reports indicate that monocyclic aromatic products (up to C_{12}) are formed on ZSM-22, but do not play an important role as active HCP species in the production of alkenes [58]. The distribution of products that were observed desorbing from the catalyst surface after a short period of ambient-pressure DME flow at 400 ℃ is generally consistent with this picture. No *hexa*-methylated aromatic products were detected, while C_6, C_7, and C_8 aromatics and cyclohexene were readily produced. Further reduction in complexity of the reaction network can be achieved by lowering the partial pressure of the methylating agent, which decreases the possible pathways involving formaldehyde [43] and slows the secondary reactions of SMS with oxygenates and hydrocarbons. Upon lowering the pressure of DME flow by eight orders of magnitude, the products no longer contained significant amounts of aromatics, instead consisting mostly of short alkenes and unreacted DME. It should be noted, however, that the negative dependency of aromatics formation on DME pressure is not straightforward. Complementary IR experiments revealed the presence of aromatic species on the catalyst surface, even after complete evacuation of the gas phase, and the amount of aromatics was surprisingly higher following 10^{-2} mbar DME pretreatment than following 10^{3} mbar DME pretreatment. We attribute this apparent disagreement between the IR and desorption/mass-spectrometry measurements to unequal pressure conditions. IR experiments with 10^{-2} mbar DME flow can be considered as an intermediate step in lowering the pre-treatment pressure from 10^{3} mbar to 10^{-6} mbar. Given the transient nature of the experiment, the amount of aromatics retained in the catalyst may depend non-monotonously on the initial DME pressure and the evacuation conditions. Nevertheless, the total concentration of adsorbed species in the IR spectrum declined as a function of the pretreatment pressure, which was intended in this study to be a means for minimization of the kinetic interference of adspecies other than surface methoxy groups (SMS).

Importantly, following prolonged evacuation at 10^{-8} mbar, the residual methylation reactivity of the catalyst towards an injected alkene was significantly higher in the case of low-pressure pretreatment. This observation can be rationalized by several co-occuring processes that may contribute to decreasing the residual reactivity during the evacuation period. The formation of SMS from DME and DME-derived methanol occurs in parallel to their consumption by: (i) C-C coupling reactions with DME and methanol to form primary alkenes and other proto-HCP species and (ii) homologation of the effusing primary alkenes and aromatics via methylation. The rates of SMS consumption reactions are significantly higher during ambient-pressure DME exposure. After the DME supply was cut-off, the effusing residual DME and product molecules continue the consumption of SMS from the catalyst surface. Furthermore, the higher-molecular weight products such as long-chain alkenes can remain trapped in ZSM-22, contributing to catalyst deactivation by blocking the active sites. This picture is supported by the IR spectra that indicate the abundance of the residual hydrocarbon species on the catalyst after evacuation (see Fig. S13) and the absence of proton recovery (see Fig. 4). Although quantitative correspondence between IR and TAP conditions could not be established, the fact that after ambient-pressure pre-treatment the catalyst exhibited very low reactivity towards an injected alkene suggests that the residual hydrocarbon species are not methylation-competent. After low-pressure DME exposure, on the other hand, the effusing product molecules are smaller in size, fewer in number, and effuse from the pores faster than after ambient-pressure DME exposure. In combination with the continuous formation of SMS from slowly-desorbing DME, as suggested by IR spectra of the ν_{OH} region (Fig. 4(a)), the low-pressure DME exposure/evacuation procedure preserves more unreacted, methylation-competent SMS than the ambient-pressure DME exposure/evacuation.

The goal of minimizing interference from various guest molecules within the micropores on the observed methylation kinetics and the goal of maximizing the coverage of SMS species amenable to kinetic characterization seem to be at odds with each other when it comes to TAP experiments with ZSM-22. The observed rate of DME desorption (Fig. 3) indicates that oxygenates are bound very strongly within the micropores of TON zeolite even at 400 °C. Omojola and co-authors have previously demonstrated that DME is much more stable on the surface of ZSM-5 than methanol [59,60]. However, their TPD as well as step-transient data, both of which were recorded under qualitatively similar sub-ambient pressures, demonstrate that DME is not nearly as stable on ZSM-5 as on ZSM-22. DME desorption from ZSM-5 peaked at 300 °C and did not exhibit significant tailing in step-response transients, while we observed very slow DME desorption from ZSM-22 at 400 °C. As already discussed above, the reactions of DME and, possibly, MTH products with SMS continue on ZSM-22 well after the supply of fresh DME is stopped due to slow DME desorption. By the time the desorption of DME and other species no longer influences the shapes of alkene methylation reactants and products, relatively little SMS remains on the surface of the catalyst. Pulse-wise addition of DME in the form of nanomolar pulses leads to a similar outcome compared to short low-pressure DME flow (see Fig. S11), as indicated by the convergent reactivities of the catalyst towards alkenes and the response shapes of methylation products.

The titration experiment (see Fig. 5) of the reference catalyst state after the low-pressure DME pre-treatment revealed that only ~ 5% of Brønsted sites were occupied by methoxy species in our kinetic measurements, which is significantly lower than the full coverage assumed in Brogaard et al. [17]. The same conclusion is supported by the prevalence of free Brønsted protons in the IR spectrum (Fig. 4). Estimated SMS coverage has two important implications for precise kinetic characterization of alkene methylation: (i) the reaction location can be ascribed to the interior of the zeolite pores and (ii) the most abundant form of adsorbed reactants can be assigned to alkenes adsorbed on free Brønsted sites as spectators. The first conclusion follows from the fact that the total amount of carbon titrated from the reference catalyst state exceeds the hypothetical amount of Brønsted acid sites on the outer surfaces of ZSM-22 crystals by at least a factor of ten (~5% vs $C_{H+,ext}/C_{H+,tot} = S_{ext}/S_{BET} = 0.5\%$). Thus, our results disagree with mechanistic proposals that assign MTH activity of ZSM-22 primarily to the active sites located near the pore mouths [61]. However, this does not contradict the substantial evidence of preferential

adsorption of long-chain branched hydrocarbons at the pore mouths [62]. The second conclusion, that SMS are in considerable minority with respect to free protons under the vacuum conditions investigated, is advantageous for quantifying the rate constants in the absence of a reliable adsorption/diffusion model for alkene transport within the catalyst. Namely, it is justified to assume that the mean residence time of alkenes within the catalyst zone during methylation experiments, which is largely controlled by adsorption, can be inferred from the kinetically "model free" concentration transients during alkene adsorption experiments with no conversion over non-methylated catalyst.

Equipped with the adsorption-controlled mean residence time, we estimated (see Table 3) the apparent first order rate constants of the alkene methylation reactions – the core objective of the present study. The rate constants observed at 400 °C in this work compare well with experimental values from Brogaard et al. [17], taking into account that adsorption on free Brønsted sites is not significant at this temperature. The rate constants reproduce the order of magnitude as well as ranking of values between homologous alkenes. In order to compare experimental activation energies to DFT-derived values, one has to consider that the initial states used for energy referencing were different between the experiments and the theory (see Fig. 7). In *ab initio* calculations, the intrinsic reaction barrier E_a^{int} was referenced to alkene pre-adsorbed on SMS, i.e. the "internal" reference state on the reaction coordinate, while the apparent barrier E_a^{app} with respect to free gas-phase alkene was offset by the adsorption enthalpy of this pre-adsorbed species ΔH_{ads}^{CH3}. In our experiments, the rate constants were evaluated with respect to an adsorbed state of alkene in the presence of an excessive amount of free protons – a pseudo-reactant – which served as a new reference state that was "external" with respect to the reaction coordinate. In order to calculate the apparent barrier for the same reference state – a gas-phase alkene – the empirical (apparent) enthalpy of adsorption for the proton-bound species ΔH_{ads}^{H+}(Table 1) was subtracted from the experimental pseudo-intrinsic reaction barrier E_a^{exp}. The resulting values of the energy-corrected apparent activation barriers are in close agreement with the theoretical apparent reaction barriers for all alkenes investigated. In particular, the apparent activation energies decrease with increasing carbon number. These experiments also reproduced the lowering of the methylation rate constant for *iso*-butene with respect to that of propene, despite the lower activation energy of *iso*-butene. This trend is consistent with the theoretically predicted lowering of the *iso*-butene pre-exponential factor due to steric hindrance of the surrounding pore.

5. Conclusions

The intrinsic kinetics of C_2-C_4 alkene methylation, which is a crucial step in the Methanol-To-Hydrocarbons (MTH) reaction, were investigated on a ZSM-22 (TON) zeolite by transient pulse-response Temporal Analysis of Products (TAP) experiments. ZSM-22 was first pretreated with DME, which established a stable population of methoxy groups on the surface. This enabled isolation of the step-wise methylation pathways from other possible reaction routes. The protocol of catalyst pretreatment with DME was tailored to ensure that only surface-bound methylation-competent species, most likely methoxy species (SMS), were present during the subsequent reactions with alkenes. We found that typical MTH products were produced during both low-pressure (~10^{-5} mbar) and ambient pressure (~10^{3} mbar) 3-minute DME treatments, but the latter resulted in higher amounts of aromatics. When the pretreated catalyst was exposed to vacuum, unreacted DME and hydrocarbon products continued to desorb for a surpris-

Table 3
Comparison of kinetic parameters to the experimental and theoretical values from Brogaard et al. [17]

	k_{app}^{673K}, 1/s		E_a^{app}, kJ/mol				
	this work	reference, experiment	this work	Reference	$E_a^{app} = E_a^{exp} - \Delta H_{ads}^{H+}$	Experiment	Theory
			E_a^{exp}	ΔH_{ads}^{H+}			
C_2H_4	45	10	110	58	**52**	–	**59**
C_3H_6	117	100	88	56	**32**	23 ± 5	**28**
i-C_4H_8	49	10	71	52	**19**	–	**15**
c-C_4H_8	271	–	65	49	**16**	–	**–**
1-C_4H_8	–	–	–	–	–	–	**20**

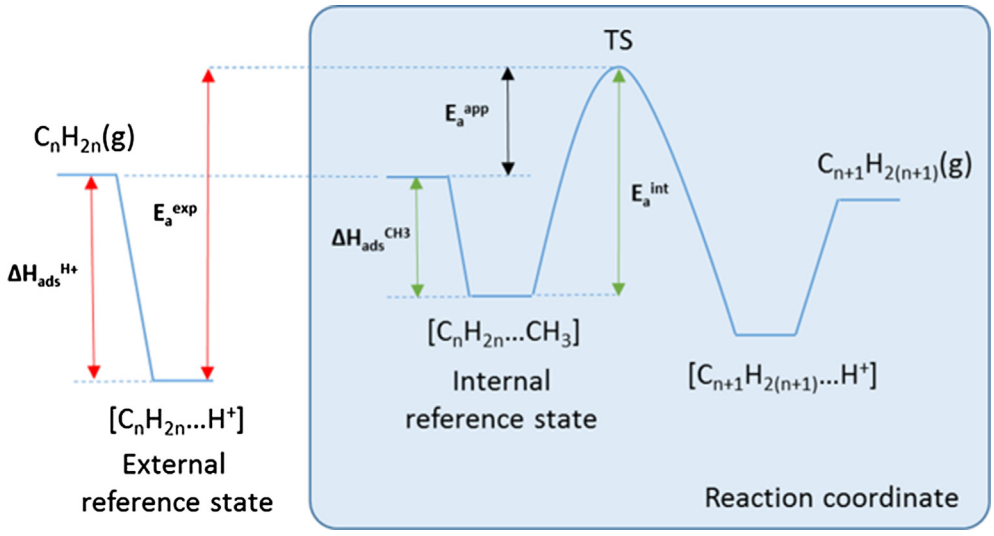

Fig. 7. Energy profile along the step-wise alkene methylation pathway in the presence of parallel adsorption of alkenes on free protons, including the definitions of apparent and intrinsic reaction barriers with respect to the "internal" and "external" reference states.

ingly long period of time, and DME could still be detected in trace amounts after 2.5 h of evacuation at 400 °C. Moreover, the residual methylation reactivity of the pretreated catalyst towards injected alkenes was drastically different after low- and ambient-pressure DME treatments. While the ambient-pressure DME-treated catalyst was practically inactive immediately after the start of evacuation, the low-pressure DME-treated catalyst exhibited a stable methylation activity even after an overnight evacuation. The amount of methoxy groups that was available for alkene methylation after this pre-treatment was equivalent to 4–6% of the total amount of Brønsted protons according to a titration experiment. Supplementary IR measurements confirmed that free protons are still present in abundance after a low-pressure DME exposure.

The established well-defined and reproducible population of SMS on the catalyst was then quantitatively reacted with nanomolar pulses of ethene, propene, *cis*-2-butene, and isobutene in the 300–400 °C temperature range. Although simple models of alkene adsorption and diffusion in zeolites were found to be inapplicable to our data, we were able to estimate the intrinsic rate constants of alkene methylation by empirically accounting for those interactions in our analysis by taking advantage of control experiments with alkenes in non-methylated zeolite and kinetically "model-free" data analysis techniques. In agreement with theoretical predictions and previously published TAP data, the rate of alkene methylation by SMS increases from ethene to propene to linear (cis-)butene. Iso-butene's methylation is hindered below that of propene due to additional steric constraints that the 10-member ring pores of the TON structure impose on its branched transition state. Adsorption-corrected apparent activation energies agree well with *ab initio* calculations.

To conclude, the present study not only reproduces the experimental results recorded on another TAP instrument [17], but also validates the theoretical model of step-wise alkene methylation in TON zeolites. The stark difference between the pools of surface species that can be prepared and kinetically characterized under ambient and low-pressure conditions highlights the potential benefit of low-pressure kinetic measurements for fundamental investigations of zeolite-mediated reactions. Unlike extensive low-pressure studies of metal and metal-oxide catalysts within the field of surface science, low-pressure studies of zeolites have not been widely reported in the literature. Our findings suggest that precise kinetic characterization of these materials under low-pressure conditions is a promising research avenue towards reconciliation of experimental data with *ab initio* calculations and rigorous single-parameter variation studies of structure-performance relationships.

Declaration of Competing Interest

The authors declare that they have no known competing financial interests or personal relationships that could have appeared to influence the work reported in this paper.

Acknowledgments

The authors acknowledge the support provided by the Research Council of Norway (NFR) through the Nanoreactor project (contract 239193). The TAP instrument was made available by the National Surface And Interface Characterization Laboratory (NICE) – part of the Norwegian national infrastructure. The authors express their gratitude to Dr. J. T. Gleaves and Mr. J. T. Gleaves Jr. of Mithra Tech. (USA), Dr. R. Fushimi of INL (USA), and technical specialists at the Departments of Chemistry and Physics (UiO) for sharing their invaluable expertise. We also thank Dr. G. S. Yablonsky (WUSTL, USA), Dr. D. Constales (Ugent, Belgium), and Mr. M. Morten (UiO) for many fruitful discussions. Ms. J. C. Child is acknowledged for her sage advice that facilitated the preparation of this manuscript.

Appendix A. Supplementary material

Supplementary data to this article can be found online at https://doi.org/10.1016/j.jcat.2020.03.020.

References

[1] J.K. Norskov, T. Bligaard, J. Rossmeisl, C.H. Christensen, Towards the computational design of solid catalysts, Nat. Chem. 1 (1) (2009) 37–46, https://doi.org/10.1038/nchem.121.
[2] E.A. Pidko, Toward the balance between the reductionist and systems approaches in computational catalysis: model versus method accuracy for the description of catalytic systems, ACS Catal. 7 (7) (2017) 4230–4234, https://doi.org/10.1021/acscatal.7b00290.
[3] M. Westgård Erichsen, K. De Wispelaere, K. Hemelsoet, S.L.C. Moors, T. Deconinck, M. Waroquier, S. Svelle, V. Van Speybroeck, U. Olsbye, How zeolitic acid strength and composition alter the reactivity of alkenes and aromatics towards methanol, J. Catal. 328 (2015) 186–196, https://doi.org/10.1016/j.jcat.2015.01.013.
[4] K.D. Wispelaere, S. Bailleul, V.V. Speybroeck, Towards molecular control of elementary reactions in zeolite catalysis by advanced molecular simulations mimicking operating conditions, Catal. Sci. Technol. 6 (8) (2016) 2686–2705, https://doi.org/10.1039/C5CY02073E.
[5] M.L. Sarazen, E. Doskocil, E. Iglesia, Effects of void environment and acid strength on alkene oligomerization selectivity, ACS Catal. 6 (10) (2016) 7059–7070, https://doi.org/10.1021/acscatal.6b02128.
[6] Introduction to Zeolite science and practice, Volume 168, Third Edition (Studies in Surface Science and Catalysis) by Jiri Cejka, Herman van Bekkum, A. Corma, F. Schueth: Elsevier Science 9780444530639 Hardcover, 3. - Ergodebooks https://www.abebooks.com/Introduction-Zeolite-science-practice-Volume-168/11792817150/bd (accessed Nov 19, 2019).
[7] X. Zhang, D. Liu, D. Xu, S. Asahina, K.A. Cychosz, K.V. Agrawal, Y.A. Wahedi, A. Bhan, S.A. Hashimi, O. Terasaki, et al., Synthesis of self-pillared zeolite nanosheets by repetitive branching, Science 336 (6089) (2012) 1684–1687, https://doi.org/10.1126/science.1221111.
[8] U. Olsbye, S. Svelle, M. Bjørgen, P. Beato, T.V.W. Janssens, F. Joensen, S. Bordiga, K.P. Lillerud, Conversion of methanol to hydrocarbons: how zeolite cavity and pore size controls product selectivity, Angew. Chem. Int. Ed. 51 (24) (2012) 5810–5831, https://doi.org/10.1002/anie.201103657.
[9] Teketel, S.; Erichsen, M. W.; Bleken, F. L.; Svelle, S.; Lillerud, K. P.; Olsbye, U. Chapter 6:Shape Selectivity in Zeolite Catalysis. The Methanol to Hydrocarbons (MTH) Reaction. In Catalysis; 2014; pp 179–217. https://doi.org/10.1039/9781782620037-00179.
[10] I. Yarulina, A.D. Chowdhury, F. Meirer, B.M. Weckhuysen, J. Gascon, Recent trends and fundamental insights in the methanol-to-hydrocarbons process, Nat. Catal. 1 (6) (2018) 398–411, https://doi.org/10.1038/s41929-018-0078-5.
[11] S. Svelle, B. Arstad, S. Kolboe, O. Swang, A theoretical investigation of the methylation of alkenes with methanol over acidic zeolites, J. Phys. Chem. B 107 (35) (2003) 9281–9289, https://doi.org/10.1021/jp022201q.
[12] I.M. Hill, S.A. Hashimi, A. Bhan, Corrigendum to "kinetics and mechanism of olefin methylation reactions over zeolites", J. Catal. 291 (2012) 155–157, https://doi.org/10.1016/j.jcat.2012.04.009.
[13] J. Van der Mynsbrugge, M. Visur, U. Olsbye, P. Beato, M. Bjørgen, V. Van Speybroeck, S. Svelle, Methylation of benzene by methanol: single-site kinetics over H-ZSM-5 and H-beta zeolite catalysts, J. Catal. 292 (2012) 201–212, https://doi.org/10.1016/j.jcat.2012.05.015.
[14] Saepurahman; Visur, M.; Olsbye, U.; Bjørgen, M.; Svelle, S. In Situ FT-IR Mechanistic Investigations of the Zeolite Catalyzed Methylation of Benzene with Methanol: H-ZSM-5 versus H-Beta. Top Catal 2011, 54 (16–18), 1293–1301. https://doi.org/10.1007/s11244-011-9751-5.
[15] K. De Wispelaere, J.S. Martínez-Espín, M.J. Hoffmann, S. Svelle, U. Olsbye, T. Bligaard, Understanding zeolite-catalyzed benzene methylation reactions by methanol and dimethyl ether at operating conditions from first principle microkinetic modeling and experiments, Catal. Today 312 (2018) 35–43, https://doi.org/10.1016/j.cattod.2018.02.042.
[16] A.J. Jones, E. Iglesia, Kinetic, spectroscopic, and theoretical assessment of associative and dissociative methanol dehydration routes in zeolites, Angew. Chem. Int. Ed. 53 (45) (2014) 12177–12181, https://doi.org/10.1002/anie.201406823.
[17] R.Y. Brogaard, R. Henry, Y. Schuurman, A.J. Medford, P.G. Moses, P. Beato, S. Svelle, J.K. Nørskov, U. Olsbye, Methanol-to-hydrocarbons conversion: the alkene methylation pathway, J. Catal. 314 (2014) 159–169, https://doi.org/10.1016/j.jcat.2014.04.006.
[18] Svelle, S.; Visur, M.; Olsbye, U.; Saepurahman; Bjørgen, M. Mechanistic Aspects of the Zeolite Catalyzed Methylation of Alkenes and Aromatics with Methanol: A Review. Top Catal. 2011, 54 (13–15), 897–906. https://doi.org/10.1007/s11244-011-9697-7.
[19] C.-M. Wang, R.Y. Brogaard, B.M. Weckhuysen, J.K. Nørskov, F. Studt, Reactivity descriptor in solid acid catalysis: predicting turnover frequencies for propene

methylation in zeotypes, J. Phys. Chem. Lett. 5 (9) (2014) 1516–1521, https://doi.org/10.1021/jz500482z.
[20] R.Y. Brogaard, C.-M. Wang, F. Studt, Methanol-alkene reactions in zeotype acid catalysts: insights from a descriptor-based approach and microkinetic modeling, *ACS Catal.* (2014), 4504-4509. 10.1021/cs5014267.
[21] J.T. Gleaves, G. Yablonsky, X. Zheng, R. Fushimi, P.L. Mills, Temporal analysis of products (TAP) – recent advances in technology for kinetic analysis of multi-component catalysts, J. Mol. Catal. A: Chem. 315 (2) (2010) 108–134, https://doi.org/10.1016/j.molcata.2009.06.017.
[22] U. Olsbye, S. Svelle, K.P. Lillerud, Z.H. Wei, Y.Y. Chen, J.F. Li, J.G. Wang, W.B. Fan, The formation and degradation of active species during methanol conversion over protonated zeotype catalysts, Chem. Soc. Rev. 44 (20) (2015) 7155–7176, https://doi.org/10.1039/C5CS00304K.
[23] J.S. Martinez-Espin, M. Mortén, T.V.W. Janssens, S. Svelle, P. Beato, U. Olsbye, New insights into catalyst deactivation and product distribution of zeolites in the methanol-to-hydrocarbons (MTH) reaction with methanol and dimethyl ether feeds, Catal. Sci. Technol. 7 (13) (2017) 2700–2716, https://doi.org/10.1039/C7CY00129K.
[24] J.S. Martinez-Espin, K. De Wispelaere, M. Westgård Erichsen, S. Svelle, T.V.W. Janssens, V. Van Speybroeck, P. Beato, U. Olsbye, Benzene Co-reaction with methanol and dimethyl ether over zeolite and zeotype catalysts: evidence of parallel reaction paths to toluene and diphenylmethane, J. Catal. 349 (2017) 136–148, https://doi.org/10.1016/j.jcat.2017.03.007.
[25] J.S. Martínez-Espín, K. De Wispelaere, T.V.W. Janssens, S. Svelle, K.P. Lillerud, P. Beato, V. Van Speybroeck, U. Olsbye, Hydrogen transfer versus methylation: on the genesis of aromatics formation in the methanol-to-hydrocarbons reaction over H-ZSM-5, ACS Catal. 7 (9) (2017) 5773–5780, https://doi.org/10.1021/acscatal.7b01643.
[26] Informatics, N. O. of D. and. NIST Chemistry WebBook https://webbook.nist.gov/chemistry/ (accessed Nov 19, 2019). https://doi.org/10.18434/T4D303.
[27] Roelant, R. Mathematical Determination of Reaction Networks from Transient Kinetic Experiments, Universiteit Gent, 2010.
[28] S.O. Shekhtman, G.S. Yablonsky, J.T. Gleaves, R. Fushimi, "State defining" experiment in chemical kinetics - primary characterization of catalyst activity in a TAP experiment, Chem. Eng. Sci. 58 (21) (2003) 4843–4859, https://doi.org/10.1016/j.ces.2003.08.005.
[29] D. Constales, G.S. Yablonsky, L. Wang, W. Diao, V.V. Galvita, R. Fushimi, Precise non-steady-state characterization of solid active materials with no preliminary mechanistic assumptions, Catal. Today 298 (2017) 203–208, https://doi.org/10.1016/j.cattod.2017.04.036.
[30] G.S. Yablonsky, D. Constales, S.O. Shekhtman, J.T. Gleaves, The Y-procedure: how to extract the chemical transformation rate from reaction-diffusion data with no assumption on the kinetic model, Chem. Eng. Sci. 62 (23) (2007) 6754–6767, https://doi.org/10.1016/j.ces.2007.04.050.
[31] E.A. Redekop, G.S. Yablonsky, D. Constales, P.A. Ramachandran, C. Pherigo, J.T. Gleaves, The Y-procedure methodology for the interpretation of transient kinetic data: analysis of irreversible adsorption, Chem. Eng. Sci. 66 (24) (2011) 6441–6452, https://doi.org/10.1016/j.ces.2011.08.055.
[32] E.A. Redekop, G.S. Yablonsky, V.V. Galvita, D. Constales, R. Fushimi, J.T. Gleaves, G.B. Marin, Momentary equilibrium in transient kinetics and its application for estimating the concentration of catalytic sites, Ind. Eng. Chem. Res. 52 (44) (2013) 15417–15427, https://doi.org/10.1021/ie400677b.
[33] M. Ross Kunz, T. Borders, E. Redekop, G.S. Yablonsky, D. Constales, L. Wang, R. Fushimi, Pulse response analysis using the Y-procedure: a data science approach, Chem. Eng. Sci. 192 (2018) 46–60, https://doi.org/10.1016/j.ces.2018.06.078.
[34] Batchu, R.; Galvita, V. V.; Alexopoulos, K.; Glazneva, Tatyana. S.; Poelman, H.; Reyniers, M.-F.; Marin, G. B. Ethanol Dehydration Pathways in H-ZSM-5: Insights from Temporal Analysis of Products. Catalysis Today 2019. https://doi.org/10.1016/j.cattod.2019.04.018.
[35] Y. Schuurman, A. Pantazidis, C. Mirodatos, The TAP-2 Reactor as an Alternative Tool for Investigating FCC Catalysts, Chem. Eng. Sci. 54 (15–16) (1999) 3619–3625, https://doi.org/10.1016/S0009-2509(98)00508-9.
[36] M. Bernauer, E. Tabor, V. Pashkova, D. Kaucký, Z. Sobalík, B. Wichterlová, J. Dedecek, Proton proximity – new key parameter controlling adsorption, desorption and activity in propene oligomerization over H-ZSM-5 zeolites, J. Catal. 344 (2016) 157–172, https://doi.org/10.1016/j.jcat.2016.09.025.
[37] F. Geobaldo, G. Spoto, S. Bordiga, C. Lamberti, A. Zecchina, Propene oligomerization on H-mordenite: hydrogen-bondinginteraction, chain initiation, propagation and hydrogen transferstudied by temperature-programmed FTIR and UV–VISspectroscopies, J. Chem. Soc., Faraday Trans. 93 (6) (1997) 1243–1249, https://doi.org/10.1039/A607052C.
[38] M. Bjørgen, K.-P. Lillerud, U. Olsbye, S. Bordiga, A. Zecchina, 1-Butene oligomerization in brönsted acidic zeolites: mechanistic insights from low-temperature in situ FTIR spectroscopy, J. Phys. Chem. B 108 (23) (2004) 7862–7870, https://doi.org/10.1021/jp0377836.
[39] Z. Liu, Y. Chu, X. Tang, L. Huang, G. Li, X. Yi, A. Zheng, Diffusion dependence of the dual-cycle mechanism for MTO reaction inside ZSM-12 and ZSM-22 zeolites, J. Phys. Chem. C 121 (41) (2017) 22872–22882, https://doi.org/10.1021/acs.jpcc.7b07374.
[40] O.P. Keipert, M. Baerns, Determination of the intracrystalline diffusion coefficients of alkanes in H-ZSM-5 Zeolite by a transient technique using the temporal-analysis-of-products (TAP) reactor, Chem. Eng. Sci. 53 (20) (1998) 3623–3634, https://doi.org/10.1016/S0009-2509(98)00174-2.
[41] A.H.J. Colaris, J.H.B.J. Hoebink, M.H.J.M. de Croon, J.C. Schouten, Intrapellet diffusivities from TAP Pulse responses via moment-based analysis, AIChE J. 48 (11) (2002) 2587–2596, https://doi.org/10.1002/aic.690481117.
[42] J. Zhang, X. Zhu, G. Wang, P. Wang, Z. Meng, C. Li, The origin of the activity and selectivity of silicalite-1 zeolite for toluene methylation to para-xylene, Chem. Eng. J. 327 (2017) 278–285, https://doi.org/10.1016/j.cej.2017.06.114.
[43] S.S. Arora, A. Bhan, The critical role of methanol pressure in controlling its transfer dehydrogenation and the corresponding effect on propylene-to-ethylene ratio during methanol-to-hydrocarbons catalysis on H-ZSM-5, J. Catal. 356 (2017) 300–306, https://doi.org/10.1016/j.jcat.2017.10.014.
[44] S. Bordiga, C. Lamberti, F. Bonino, A. Travert, F. Thibault-Starzyk, Probing zeolites by vibrational spectroscopies, Chem. Soc. Rev. 44 (20) (2015) 7262–7341, https://doi.org/10.1039/C5CS00396B.
[45] L. Palumbo, F. Bonino, P. Beato, M. Bjørgen, A. Zecchina, S. Bordiga, Conversion of methanol to hydrocarbons: spectroscopic characterization of carbonaceous species formed over H-ZSM-5, J. Phys. Chem. C 112 (26) (2008) 9710–9716, https://doi.org/10.1021/jp800762v.
[46] D. Verboekend, A.M. Chabaneix, K. Thomas, J.-P. Gilson, J. Pérez-Ramírez, Mesoporous ZSM-22 zeolite obtained by desilication: peculiarities associated with crystal morphology and aluminium distribution, CrystEngComm 13 (10) (2011) 3408, https://doi.org/10.1039/c0ce00966k.
[47] Freitas, C.; Barrow, N. S.; Zholobenko, V. Accessibility and Location of Acid Sites in Zeolites as Probed by Fourier Transform Infrared Spectroscopy and Magic Angle Spinning Nuclear Magnetic Resonance https://www.ingentaconnect.com/content/matthey/jmtr/2018/00000062/00000003/art00005;jsessionid=29and75bk3l6q.x-ic-live-03 (accessed Dec 6, 2019). https://doi.org/info:doi/10.1595/205651318X696792.
[48] M.L. Sarazen, E. Iglesia, Stability of bound species during alkene reactions on solid acids, PNAS 114 (20) (2017) E3900–E3908, https://doi.org/10.1073/pnas.1619557114.
[49] R. Batchu, V.V. Galvita, K. Alexopoulos, K. Van der Borght, H. Poelman, M.-F. Reyniers, G.B. Marin, Role of intermediates in reaction pathways from ethene to hydrocarbons over H-ZSM-5, Appl. Catal. A 538 (2017) 207–220, https://doi.org/10.1016/j.apcata.2017.03.013.
[50] K. Alexopoulos, M. John, K. Van der Borght, V. Galvita, M.-F. Reyniers, G.B. Marin, DFT-based microkinetic modeling of ethanol dehydration in H-ZSM-5, J. Catal. 339 (2016) 173–185, https://doi.org/10.1016/j.jcat.2016.04.020.
[51] T.A. Nijhuis, L.J.P. van den Broeke, M.J.G. Linders, J.M. van de Graaf, F. Kapteijn, M. Makkee, J.A. Moulijn, Measurement and modeling of the transient adsorption, desorption and diffusion processes in microporous materials, Chem. Eng. Sci. 54 (20) (1999) 4423–4436, https://doi.org/10.1016/S0009-2509(99)00131-1.
[52] J.A. Delgado, T.A. Nijhuis, F. Kapteijn, J.A. Moulijn, Determination of adsorption and diffusion parameters in zeolites through a structured approach, Chem. Eng. Sci. 59 (12) (2004) 2477–2487, https://doi.org/10.1016/j.ces.2004.03.013.
[53] B.A. De Moor, M.-F. Reyniers, O.C. Gobin, J.A. Lercher, G.B. Marin, Adsorption of C2–C8 N-alkanes in zeolites, J. Phys. Chem. C 115 (4) (2011) 1204–1219, https://doi.org/10.1021/jp106536m.
[54] P. Cnudde, K. De Wispelaere, J. Van der Mynsbrugge, M. Waroquier, V. Van Speybroeck, Effect of temperature and branching on the nature and stability of alkene cracking intermediates in H-ZSM-5, J. Catal. 345 (2017) 53–69, https://doi.org/10.1016/j.jcat.2016.11.010.
[55] C.M. Nguyen, B.A. De Moor, M.-F. Reyniers, G.B. Marin, Isobutene protonation in H-FAU, H-MOR, H-ZSM-5, and H-ZSM-22, J. Phys. Chem. C 116 (34) (2012) 18236–18249, https://doi.org/10.1021/jp304081k.
[56] Z.-M. Cui, Q. Liu, Z. Ma, S.-W. Bian, W.-G. Song, Direct observation of olefin homologations on zeolite ZSM-22 and Its Implications To Methanol To Olefin Conversion, J. Catal. 258 (1) (2008) 83–86, https://doi.org/10.1016/j.jcat.2008.05.029.
[57] M. Dyballa, P. Becker, D. Trefz, E. Klemm, A. Fischer, H. Jakob, M. Hunger, Parameters influencing the selectivity to propene in the MTO conversion on 10-Ring zeolites: directly synthesized zeolites ZSM-5, ZSM-11, and ZSM-22, Appl. Catal. A 510 (2016) 233–243, https://doi.org/10.1016/j.apcata.2015.11.017.
[58] S. Teketel, U. Olsbye, K.-P. Lillerud, P. Beato, S. Svelle, Selectivity control through fundamental mechanistic insight in the conversion of methanol to hydrocarbons over zeolites, Microporous Mesoporous Mater. 136 (1–3) (2010) 33–41, https://doi.org/10.1016/j.micromeso.2010.07.013.
[59] T. Omojola, N. Cherkasov, A.I. McNab, D.B. Lukyanov, J.A. Anderson, E.V. Rebrov, A.C. van Veen, Mechanistic insights into the desorption of methanol and dimethyl ether over ZSM-5 catalysts, Catal. Lett. 148 (1) (2018) 474–488, https://doi.org/10.1007/s10562-017-2249-4.
[60] T. Omojola, D.B. Lukyanov, A.C. van Veen, Transient kinetic studies and microkinetic modeling of primary olefin formation from dimethyl ether over ZSM-5 catalysts, Int. J. Chem. Kinet. 51 (7) (2019) 528–537, https://doi.org/10.1002/kin.21275.
[61] F.-F. Wei, Z.-M. Cui, X.-J. Meng, C.-Y. Cao, F.-S. Xiao, W.-G. Song, Origin of the low olefin production over HZSM-22 and HZSM-23 zeolites: external acid sites and pore mouth catalysis, ACS Catal. 4 (2) (2014) 529–534, https://doi.org/10.1021/cs400855p.
[62] R.A. Ocakoglu, J.F.M. Denayer, G.B. Marin, J.A. Martens, G.V. Baron, Tracer chromatographic study of pore and pore mouth adsorption of linear and monobranched alkanes on ZSM-22 Zeolite, J. Phys. Chem. B 107 (1) (2003) 398–406, https://doi.org/10.1021/jp0264533.